



# CHORUS

This is the accepted manuscript made available via CHORUS. The article has been published as:

## Switchable valley filter based on a graphene p-n junction in a magnetic field

T. Sekera, C. Bruder, E. J. Mele, and R. P. Tiwari

Phys. Rev. B **95**, 205431 — Published 23 May 2017

DOI: [10.1103/PhysRevB.95.205431](https://doi.org/10.1103/PhysRevB.95.205431)

# Switchable valley filter based on a graphene $p$ - $n$ junction in a magnetic field

T. Sekera\*,<sup>1</sup> C. Bruder,<sup>1</sup> E.J. Mele,<sup>2</sup> and R.P. Tiwari<sup>1,3</sup>

<sup>1</sup>*Department of Physics, University of Basel, Klingelbergstrasse 82, CH-4056 Basel, Switzerland*

<sup>2</sup>*Department of Physics and Astronomy, University of Pennsylvania, Philadelphia PA 19104, USA*

<sup>3</sup>*Department of Physics, McGill University, 3600 rue University, Montreal, Quebec, Canada H3A 2T8*

(Dated: May 3, 2017)

Low-energy excitations in graphene exhibit relativistic properties due to the linear dispersion relation close to the Dirac points in the first Brillouin zone. Two of the Dirac points located at opposite corners of the first Brillouin zone can be chosen as inequivalent, representing a new *valley* degree of freedom, in addition to the charge and spin of an electron. Using the valley degree of freedom to encode information has attracted significant interest, both theoretically and experimentally, and gave rise to the field of *valleytronics*. We study a graphene  $p$ - $n$  junction in a uniform out-of-plane magnetic field as a platform to generate and controllably manipulate the valley polarization of electrons. We show that by tuning the external potential giving rise to the  $p$ - $n$  junction we can switch the current from one valley polarization to the other. We also consider the effect of different types of edge terminations and present a setup, where we can partition an incoming valley-unpolarized current into two branches of valley-polarized currents. The branching ratio can be chosen by changing the location of the  $p$ - $n$  junction using a gate.

PACS numbers: 81.05.ue, 73.40.-c, 73.43.-f

## I. INTRODUCTION

Two-dimensional (2D) materials are promising candidates for future electronics due to their unique characteristics. The pioneering 2D material, graphene, was experimentally isolated in 2004<sup>1</sup>. The bandstructure of  $p_z$  electrons in single-layer graphene, modeled as a honeycomb lattice with lattice constant  $a = 0.246$  nm consisting of two triangular Bravais sublattices  $A$  and  $B$  with nearest-neighbor hopping in the tight-binding formulation, hosts six Dirac cones resulting from touching of the valence and conduction bands at the Fermi energy  $E = 0$ . Two of the cones located at diagonally opposite corners of the first Brillouin zone can be chosen as inequivalent, for example at  $K = 2\pi/3a$  and  $-K$ . For the low-energy electronic excitations in the system they represent a new degree of freedom of an electron, in addition to the charge and spin. This *valley* degree of freedom can be exploited in analogy with the spin in spintronics, which gave rise to the field called *valleytronics*, where one uses the valley degree of freedom to encode information.

There is a strong motivation to generate, controllably manipulate and read out states of definite valley polarization, and a substantial amount of theoretical and experimental work has been done towards achieving these goals. A recent review of some advances made in the field of valleytronics in 2D materials is provided in Ref. 2. To mention some: a gated graphene quantum point contact with zigzag edges was proposed to function as a valley filter<sup>3</sup>. Superconducting contacts were shown to enable the detection of the valley polarization in graphene<sup>4</sup>. In 2D honeycomb lattices with broken inversion symmetry,

e.g. transition metal dichalcogenide (TMD) monolayers, a non-zero Berry curvature carries opposite signs in the  $K$  and  $-K$  valleys. In these 2D materials, the velocity in the direction perpendicular to an applied in-plane electric field is proportional to this Berry curvature<sup>5</sup>. Hence the electrons acquire a valley-antisymmetric transverse velocity leading to the valley Hall effect, which spatially separates different valley states. In a system where the occupation numbers of the two valleys are different (valley-polarized system), a finite transverse voltage across the sample is developed and the sign of this voltage can be used to measure the valley polarization<sup>6</sup>. The valley Hall effect can also be exploited in a biased bilayer graphene, where the out-of-plane electric field breaks the inversion symmetry<sup>7-9</sup>. Moreover, it was shown that the broken inversion symmetry results in the valley-dependent optical selection rule, which can be used to selectively excite carriers in the  $K$  or  $-K$  valley via right or left circularly polarized light, respectively<sup>10,11</sup>. Valley polarization can also be achieved in monolayer<sup>12-15</sup> and bilayer<sup>15</sup> graphene systems with barriers. In addition, proposals exploiting strain that induces pseudomagnetic fields acting oppositely in the two valleys<sup>16,17</sup> together with artificially induced carrier mass and spin-orbit coupling<sup>18</sup> have been put forward.

In this paper we propose a way to generate and controllably manipulate the valley polarization of electrons in a graphene  $p$ - $n$  junction in the presence of an out-of-plane magnetic field. Applying an out-of-plane magnetic field to the graphene sheet leads to the formation of low-energy relativistic Landau levels (LLs)<sup>19</sup>. These are responsible for the unusual quantum Hall conductance quantization  $G_n = 2_s \times 2_v \times (n + 1/2)e^2/h$ , where the integer  $n$  is the highest occupied Landau level index (for  $n$ -type doping) for a given chemical potential. The factor  $2_s$  in the formula accounts for the spin degeneracy and

---

\*Correspondence address: tiber.sekera@unibas.ch

the second factor  $2_v$  for the valley degeneracy of the Landau levels. The presence of the  $E = 0$  Dirac point and particle-hole symmetry lead to a special  $n = 0$  LL, which is responsible for the fraction  $1/2$  in the conductance.

Semiclassically, charged particles propagating in a spatially varying out-of-plane magnetic field in 2D may exhibit snake-like trajectories that are oriented perpendicularly to the field gradient<sup>20</sup>. The simplest case occurs along a nodal line of a spatially varying magnetic field<sup>21–24</sup>. Another system, a graphene  $p$ - $n$  junction in a homogeneous out-of-plane magnetic field, hosts similar states located at the interface between  $n$ - and  $p$ -doped regions. These interface states are also called snake states due to the shape of their semiclassical trajectories<sup>25–27</sup>. A correspondence between these two kinds of snake trajectories was pointed out in Ref. 28. A mapping between these two systems was found by rewriting both problems in a Nambu (doubled) formulation<sup>29</sup>. In this paper we consider a graphene  $p$ - $n$  junction in a homogeneous out-of-plane magnetic field, a system which has attracted a lot of attention<sup>30–36</sup>. In the limit of a large junction (where the phase coherence is suppressed due to inelastic scattering or random time-dependent electric fields), the conductance is a series conductance of  $n$ - and  $p$ -doped regions<sup>37</sup>. However, for sufficiently small junctions the conductance depends on the microscopic edge termination close to the  $p$ - $n$  interface. When the chemical potential in the  $n$  and  $p$  regions is within the first Landau gap, i.e., is restricted to energy values smaller than the absolute value of the energy difference between the zeroth and the first Landau level, an analytical formula for the conductance can be derived<sup>38</sup>, see Eq. (2).

We demonstrate that a three-terminal device like the one shown in Fig. 1 can be used as a switchable, i.e. voltage-tunable valley filter. In short, it works as follows: valley-unpolarized electrons injected from the upper lead are collected in the lower leads with high valley polarization. The valley polarization of the collected electrons is controlled by switching the  $p$ - $n$  junction on and off, while the partitioning of the electron density between the two lower leads is controlled by the edge termination and the width  $W$  of the central region close to the  $p$ - $n$  interface.

Our results are not restricted to graphene. They apply also to honeycomb lattices with broken inversion symmetry, where the inversion symmetry breaking term is represented by a staggered sublattice potential. As long as the amplitude of this term is smaller than the built-in potential step in the  $p$ - $n$  junction, our results remain valid. In a system with broken inversion symmetry, a non-zero Berry curvature would give rise to the valley Hall effect which could be used to read out the polarization of the outgoing states<sup>6</sup>.

The rest of this article is organized as follows. In Sec. II we describe the setup of the proposed switchable valley filter and the methods we use to investigate its properties in detail. In Sec. III we present our numerical results, which demonstrate the valley-polarized electronic transport. In Sec. IV we study the effect of poten-

tial step height and different edge terminations of the graphene lattice close to the  $p$ - $n$  interface on the valley polarization. We show that using a tilted staircase edge  $p$ - $n$  junction allows to partition a valley-unpolarized incoming current into two outgoing currents with opposite valley polarizations, where the partitioning can be controlled by tuning the location of the  $p$ - $n$  junction. Finally we summarize our results in Sec. V.

## II. SETUP

Figure 1 shows the three-terminal device that we would like to study. A rectangular region of width  $W$  and length  $L$  represents the graphene  $p$ - $n$  junction in a uniform out-of-plane magnetic field, also referred to as the scattering region. It is described by a tight-binding Hamiltonian of the form

$$H = \sum_i V(\mathbf{r}_i) c_i^\dagger c_i + \sum_{\langle i,j \rangle} t e^{i\varphi_{ij}} c_i^\dagger c_j, \quad (1)$$

where  $V(\mathbf{r}_i)$  is the scalar on-site potential at site  $i$  with coordinate  $\mathbf{r}_i$  and  $\varphi_{ij} = (e/\hbar) \int_i^j \mathbf{A} \cdot d\mathbf{r}$  is the Peierls phase accumulated along the link from site  $i$  to site  $j$  in magnetic field  $\mathbf{B} = [0, 0, B]$ . The Zeeman splitting is neglected, i.e., we consider spinless electrons. The sum over  $\langle i, j \rangle$  denotes the sum over nearest neighbors. We choose the Landau gauge, where the vector potential is

$$\mathbf{A} = [0, Bx, 0].$$

In this gauge we can define a (quasi-)momentum parallel to the edges of the leads. The leads  $L_0$ ,  $L_1$ , and  $L_2$  are modeled as semi-infinite zigzag nanoribbons, where the valley index can be well distinguished in  $k$ -space. They are also described by the Hamiltonian (1) and below we present the case with  $B = 0$  in the leads, which is however not crucial for our results. The Peierls phase  $\varphi_{ij}$  can be written in the form

$$\varphi_{ij} = 2\pi \frac{\phi}{\phi_0} \frac{2}{\sqrt{3}a^2} \frac{x_i + x_j}{2} (y_j - y_i),$$

where  $\phi_0 = h/e$  is the magnetic flux quantum and  $\phi = BS$  is the flux through a single hexagonal plaquette of a honeycomb lattice. Here,  $S = \sqrt{3}a^2/2$  is the area of a hexagonal plaquette of the honeycomb lattice. An important length scale derived from magnetic field is the magnetic length  $\ell_B = \sqrt{\hbar/eB}$ . In the rest of the paper the magnetic field is chosen such that  $\phi/\phi_0 = 0.003$  and hence  $\ell_B \approx 6.78a$ . We also denote the energy difference between the first and the zeroth LL by  $\delta = \sqrt{2}\hbar v_F/\ell_B = 0.18t$ , where the Fermi velocity at the  $K$  point is  $v_F = \sqrt{3}at/2\hbar$ .

The scalar on-site potential is varying only in the  $x$ -direction as

$$V(x) = V_0 \tanh(x/\ell),$$

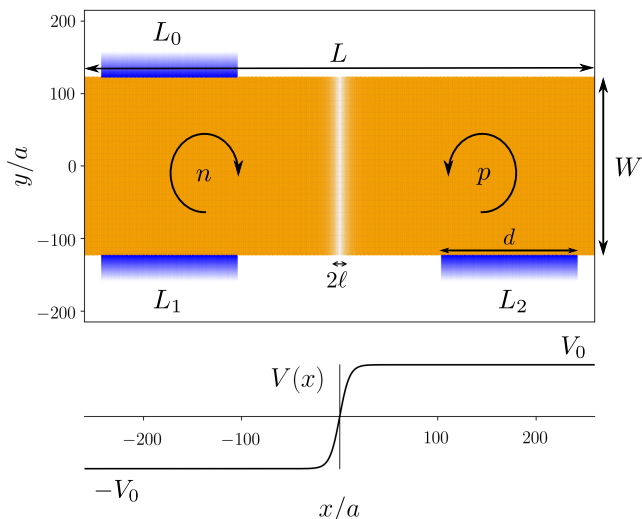


FIG. 1: Three-terminal device used as a switchable valley filter. The three leads of horizontal size  $d$  with zigzag edge termination, upper lead  $L_0$ , lower-left lead  $L_1$  and lower-right lead  $L_2$ , are attached to the rectangular scattering region of length  $L$  and width  $W$ . Top and bottom edges of the scattering region are of armchair type, while the left and right edges are of zigzag type. The  $p$ - $n$  interface of thickness  $2\ell$  (white color gradient) is modeled by an  $x$ -dependent on-site potential  $V(x)$ . In an out-of-plane magnetic field with  $n$  Landau levels occupied ( $n = 0, 1, 2, \dots$ ), there are  $2n + 1$  edge states with opposite chirality in the  $n$ - and  $p$ -doped region. Along the  $p$ - $n$  interface there are  $2(2n + 1)$  co-propagating snake states.

where  $V_0$  is the external scalar potential and  $2\ell$  is the thickness of the domain wall characterizing the  $p$ - $n$  junction. If both  $V_0$  and  $B$  are non-zero and  $V_0 < \delta$  in such a setup, there exist two snake states co-propagating along the  $p$ - $n$  junction<sup>29</sup>. The orientation of the fields in the system is such that the snake states are traveling downwards in the negative  $y$ -direction.

We calculate the transmission  $T_{10}$  from  $L_0$  to  $L_1$ , and  $T_{20}$  from  $L_0$  to  $L_2$ . We also calculate the valley-resolved transmissions, with the following notation:  $T_{20}^{K(-K)}$  is the transmission from  $L_0$  to  $L_2$ , where in  $L_2$  we sum only over outgoing modes with  $k \in (0, \pi/a]$  ( $k \in (-\pi/a, 0]$ ). Then we can define the valley polarization in  $L_2$  as  $P_2 = (T_{20}^K - T_{20}^{-K})/T_{20}$ . Analogous quantities are defined for  $L_1$ .

Due to the absence of backscattering in chiral quantum Hall edge states and the symmetry of the  $p$ - $n$  junction for  $E = 0$ , the net transmission (no spin) is  $T_{10} + T_{20} = 2n + 1$ , where  $n$  is the highest occupied LL in the  $n$ -doped region. The partitioning of the net transmission between  $T_{10}$  and  $T_{20}$  depends on the edge termination close to the  $p$ - $n$  interface according to the formula<sup>38</sup>

$$T_{20} = \frac{1}{2}(1 - \cos \Phi), \quad (2)$$

where  $\Phi$  is the angle between valley isospins at the upper and lower edge represented as vectors on the Bloch

sphere. For armchair edges one has  $\Phi = \pi$  if  $W/a \bmod 3 = 0$  and  $\Phi = \pm\pi/3$  otherwise. The formula is valid if the  $n$  and  $p$  regions are on the lowest Hall plateau, where the quantum Hall conductances in the  $n$ - and  $p$ -doped regions are equal to  $e^2/h$  (ignoring the spin degree of freedom)<sup>38</sup>. The transmission from  $L_0$  to  $L_1$  is then given by  $T_{10} = 1 - T_{20}$ . Interference between wavefunctions of the snake states is responsible for this partitioning. The snake-state wavefunctions are located at the  $p$ - $n$  interface and their effective spread in the  $x$ -direction is given by the magnetic length  $\ell_B$  to the left and right of the interface. Hence one way to control the partitioning experimentally will be to control the edge termination around the  $p$ - $n$  interface on a length scale of the order of  $2\ell_B$ .

In the following we show numerically that by switching the  $p$ - $n$  junction on ( $V_0 \neq 0$ ) and off ( $V_0 = 0$ ) we can control the valley polarization of the outgoing states in leads  $L_1$  and  $L_2$ .

### III. SWITCHABLE VALLEY FILTER

We demonstrate the principle of the switchable valley filter using a  $p$ - $n$  junction in an out-of-plane magnetic field, where the upper and the lower edges are of armchair type. The system is described by the Hamiltonian shown in Eq. (1). The width  $W$  of the  $p$ - $n$  junction is chosen such that the number of hexagons in this width is a multiple of 3, i.e. such that the corresponding armchair nanoribbon would be metallic. If, furthermore, both the  $n$ - and  $p$ -doped regions are on the lowest Hall plateau and  $V_0$  is large enough<sup>38</sup>, we expect  $T_{20} = 1$  and  $T_{10} = 0$ , see Eq. (2). The switchable valley filter is based on the fact that for a zigzag graphene nanoribbon the quantum Hall edge states of the  $n = 0$  LL lying in opposite valleys  $K$  and  $-K$  have opposite velocities<sup>19,39,40</sup>.

Unless stated otherwise, the system has length  $L = 520a$  and width  $W = 246a$  (the exception is Fig. 4). The horizontal size of each lead is  $d = 156a$ . The thickness of the  $p$ - $n$  junction is  $2\ell = 20a$ . We set the magnitude of the magnetic field in the leads to zero, which is however not crucial for the result. Our tight-binding calculations were performed using Kwant<sup>41</sup>.

First, we consider the case  $V_0 = 0$ . A valley-unpolarized electron current (injected from both valleys) in  $L_0$  ends up as outgoing valley-polarized electron current in  $L_2$ . In Figs. 2(a) and 3(a) we also plot the probability density of one of the states carrying the current by drawing a black dot on each site whose size is proportional to the probability of finding an electron on that particular site. This is plotted for a state in the scattering region due to an incoming mode from  $L_0$  at Fermi energy  $E$  and with momentum  $k_y$  indicated by the red arrow in the bandstructure for  $L_0$ , see Figs. 2(b) and 3(b). Figure 2(a) shows the probability density of the state in the scattering region due to an incoming mode from  $L_0$  at  $E = \delta/2$  and  $k_y a = 2.08$ . Since  $V_0 = 0$ , there are no

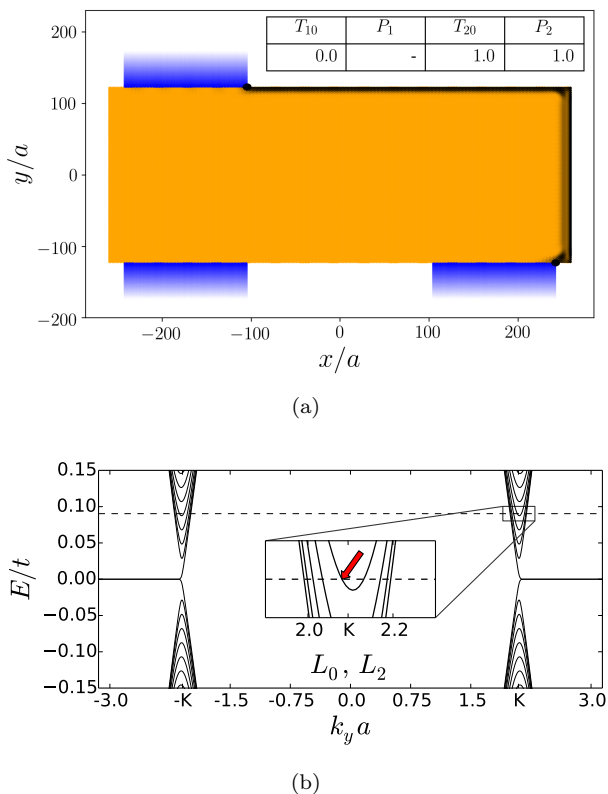


FIG. 2: Case when  $V_0 = 0$  and  $E = \delta/2$ . (a) State in the scattering region due to incoming mode from lead  $L_0$  with  $k_y a = 2.08$ . The inset table lists the transmissions  $T_{10}$  and  $T_{20}$  and polarizations  $P_1$  and  $P_2$ . (b) Bandstructure of leads  $L_0$  and  $L_2$ . The Fermi energy is indicated by the horizontal dashed line. The red arrow indicates the incoming mode on lead  $L_0$  which has velocity  $v < 0$  and is chosen to be plotted in (a).

snake states in this system and the electronic current is carried by the quantum Hall edge states. The electrons injected from  $L_0$  travel in a clockwise manner to  $L_2$ . The calculated transmissions  $T_{10}$  and  $T_{20}$  and polarizations  $P_1$  and  $P_2$  are shown in the inset table in Fig. 2(a). We find that the outgoing electrons in  $L_2$  are perfectly polarized in the  $K$  valley. This shows the valley-polarized nature of the zeroth LL. Thus, this system can be used as a valley filter.

If we now turn on the  $p$ - $n$  junction, the situation will change. We assume that the  $p$ - $n$  junction is turned on adiabatically. We choose  $V_0 = \delta/2$ , so that the  $n$ - and  $p$ -doped regions are on the  $n = 0$  LL. Figure 3(a) shows the probability density of the state in the scattering region due to the incoming mode from  $L_0$  at the Fermi energy  $E = 0.001t$  and with  $k_y a = 2.08$  (red arrow in the inset of Fig. 3(b)). In this system there are two co-propagating snake states along the  $p$ - $n$  interface, and the electronic current is carried by these states. These snake states are located at the  $p$ - $n$  interface and spread in the  $\pm x$ -direction over the magnetic length  $l_B$ , which is independent of the domain wall thickness  $2\ell$ .

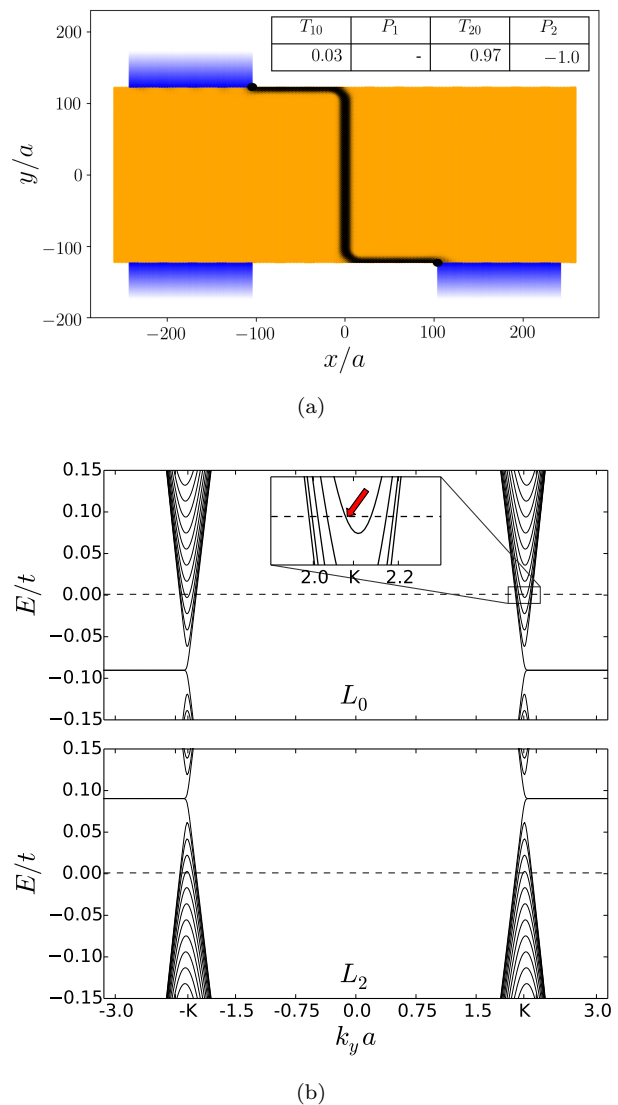


FIG. 3: Case when  $V_0 = \delta/2$  and  $E = 0.001t$ . (a) State in the scattering region due to incoming mode from lead  $L_0$  with  $k_y a = 2.08$ . The inset table lists the transmissions  $T_{10}$  and  $T_{20}$  and polarizations  $P_1$  and  $P_2$ . (b) Top: bandstructure of lead  $L_0$ . The Fermi energy is indicated by the horizontal dashed line. The red arrow indicates the incoming mode chosen to plot (a). Bottom: bandstructure of lead  $L_2$ .

The electrons injected from  $L_0$  now travel along the upper edge in the  $n$  region towards the  $p$ - $n$  interface and continue along the  $p$ - $n$  interface towards the lower edge, where they enter the  $p$  region with probability  $\approx 1$  due to the specifically chosen  $W$  and the armchair edge termination at both ends of the interface. Finally, they end up in  $L_2$ . The corresponding transmissions and polarizations are shown in the inset table of Fig. 3(a). We find that the electrons in  $L_2$  are nearly perfectly polarized in the  $-K$  valley. Thus, by turning on the  $p$ - $n$  junction we have *flipped* the valley polarization of the electronic current in  $L_2$ .

It is worth noting that these results are robust with re-

spect to edge disorder because of the absence of backscattering in the chiral quantum Hall edge states. Our results also apply to the case where the magnetic field is present in the leads. However, since for low energies and dopings, only the  $n = 0$  LL plays a role, states in the leads are already valley-polarized edge states and thus our three-terminal device would then work as a perfect valley switch.

#### IV. POLARIZATIONS AND TRANSMISSIONS UPON VARYING $V_0$ AND GEOMETRY

In the following we analyze how the valley polarizations  $P_1$  and  $P_2$  and transmissions  $T_{10}$  and  $T_{20}$  change upon varying  $V_0$  and edge terminations.

*Polarization vs.  $V_0$ .* In Fig. 4 we plot the polarization in the leads as a function of  $V_0$ . Let us focus on  $P_2$ , because the majority of electrons are traveling into lead  $L_2$  (for this specifically chosen scattering region). The case shown in Fig. 2 corresponds to  $V_0 = 0$ , where  $P_2 = 1$  (not visible in the figure). For  $V_0 > 0$  (Fig. 3), the polarization in lead  $L_2$  changes sign,  $P_2 = -1$ . For  $0 < V_0 < \delta = 0.18t$  only the  $n = 0$  LL valley-polarized edge states contribute to the transport and  $P_2$  stays close to  $-1$  until  $V_0 \approx \delta$ . For  $V_0 > \delta$  the higher LLs get occupied. Edge states in the higher LLs are not valley-polarized which reduces  $P_2$ . On further increasing  $V_0$  higher and higher LLs get occupied which further obscures the edge state valley polarization of the  $n = 0$  LL and the magnitude of  $P_2$  decreases. The population of the LLs can be seen from  $T_{10} + T_{20}$  as a function of  $V_0$ , which is shown with the red curve in Fig. 4. Hence the efficiency of the switchable valley filter device is observed to decrease with an increase in  $V_0$ , i.e. with populating higher LLs.

Furthermore, one can notice in Fig. 4 that the valley polarizations  $P_1$  and  $P_2$  in leads  $L_1$  and  $L_2$  jump at the same voltages  $V_0$ , where the  $p$ - $n$  junction undergoes quantum Hall transitions and the total transmission  $T_{10} + T_{20}$  changes by 2. The larger  $V_0$ , the more the values of  $V_0$  at which the total transmission changes by 2 deviate from the vertical lines indicating the LL energies at  $E_n = \sqrt{2n}\hbar v_F/\ell_B$ . This is due to the nonlinearity of the dispersion which leads to a change in group velocity. The oscillations seen in the blue and green curves stem from oscillations of transmissions as shown in Fig. 5. This can be viewed as a consequence of interference effects between modes confined at the  $p$ - $n$  interface with different momenta<sup>36,42</sup>. However, the amplitude of these oscillations decreases with increasing system size. In our simulations, the system size is increased proportionally, i.e. parameters  $L, W, d$  and  $\ell$  are multiplied by  $\alpha = 1, 1.5, 4$ , while the magnetic flux per plaquette is kept constant,  $\phi/\phi_0 = 0.003$  (see Fig. 5).

*Different edge terminations.* We find that different edge terminations and  $p$ - $n$  interface length have almost no influence on the valley polarization in the leads, but they determine the partitioning of the net transmission

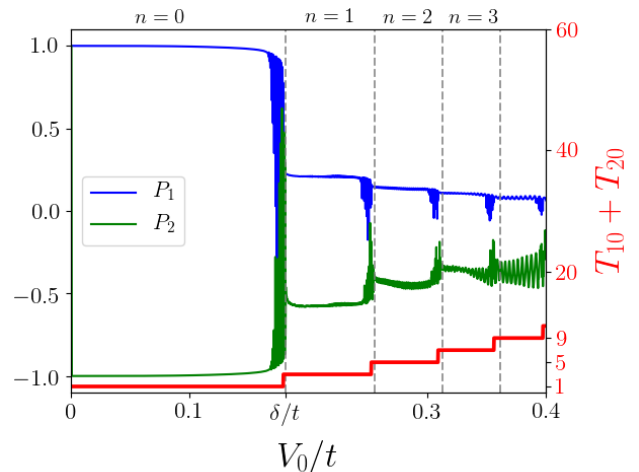


FIG. 4: Polarization  $P_1$  in lead  $L_1$  (blue, left axis), and  $P_2$  in lead  $L_2$  (green, left axis) as a function of  $V_0$  for the device shown in Fig. 1. For  $0 < V_0 < \delta$  only the  $n = 0$  Landau level (LL) is occupied and  $P_2 \approx -1$ . As soon as higher LLs get involved ( $V_0 > \delta$ ), where the edge states are not valley-polarized, the valley polarization in  $L_1$  and  $L_2$  decreases towards 0 with increasing  $V_0$ . The sum of the transmissions  $T_{10} + T_{20}$  (red step-like curve, right axis) exhibits quantization due to LLs in the scattering region. The device is a good valley filter for  $V_0 < \delta$ , i.e., when only the  $n = 0$  LL is occupied. Vertical (grey dashed) lines mark the LL energies  $E_n = \sqrt{2n}\hbar v_F/\ell_B$  in the  $n$ -doped region calculated for a linear Dirac dispersion. The parameters chosen for this figure are  $L = 2080a$ ,  $W = 984a$ ,  $\ell = 40a$ , and  $d = 320a$ .

between  $T_{10}$  and  $T_{20}$ . In Tab. I(a), where the  $p$ - $n$  interface meets armchair edges,  $T_{10}$  and  $T_{20}$  exhibit the expected periodicity when changing the width  $W$  such that the number of hexagons across the width of the scattering region changes by 3. The case in which the  $p$ - $n$  interface meets zigzag edges is considered in Tab. I(b). Here, the transmissions  $T_{10}$  and  $T_{20}$  switch values depending on whether the two edges are in zigzag or anti-zigzag configuration, which is in agreement with Ref. 43. To model different edge terminations, we also added a triangular region to the sample, see Tab. I(c)–(e) (a zoom-in onto the tip is shown in the last column of Tab. I(c)). Thus by controlling the edge termination on a length scale of  $2\ell_B$  around the  $p$ - $n$  interface one can tune the partitioning of the current into  $L_1$  and  $L_2$ . The currents in both of these leads are polarized in opposite valleys. Thus if one chooses the situation where the current is finite in both  $L_1$  and  $L_2$  (for example the case shown in Tab. I(c)), one can create two streams of oppositely valley-polarized currents in leads  $L_1$  and  $L_2$ .

*Tilted staircase edge.* Now we consider the three-terminal setup shown in Fig. 6. The upper edge has many steps on the atomic scale, shown in the upper panel of Fig. 6. The size of each of these steps is assumed to be constant and is denoted by  $\ell_{\text{step}}$ . The bottom-edge termination of the sample is of armchair type. We

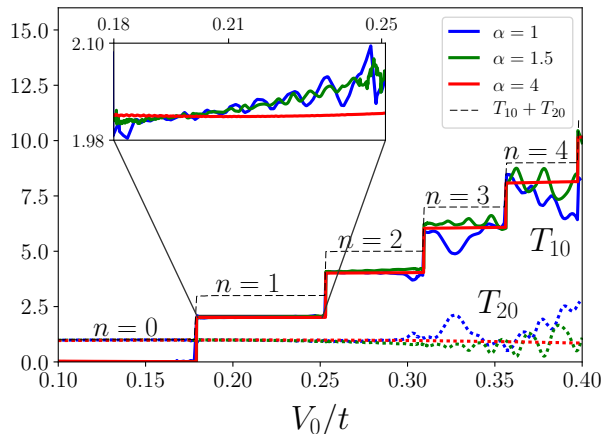


FIG. 5: Transmissions  $T_{10}$  (solid lines),  $T_{20}$  (dotted lines) and  $T_{10} + T_{20}$  (dashed line) as a function of  $V_0$  for different system sizes. The inset shows that the amplitude of the oscillations tend to vanish as we increase the system size, which is accomplished by multiplying the parameters  $L, W, d$  and  $\ell$  by a factor of  $\alpha = 1$  (blue), 1.5 (green), 4 (red) while  $\phi/\phi_0 = 0.003$  is kept constant.

study the transmission  $T_{20}$  as a function of the position of the  $p$ - $n$  interface  $x_0$ . Note that  $T_{10} = 1 - T_{20}$ , because here the parameters are such that only the  $n = 0$  LL contributes to the electronic transport. If  $\ell_{\text{step}} \gg 2\ell_B$ , the transmission  $T_{20}$  shows a plateau-like behavior (see Fig. 7(a)). The transmission jumps to a different plateau as a new step is encountered while moving  $x_0$  from  $-180a$  to  $180a$  (the jump happens on length scales of the order of  $2\ell_B$ ). Since the upper and the lower edges are of armchair type, we observe three plateau values corresponding to different angles the between valley isospins at the two edges  $\Phi = \pi, \pm\pi/3$ , in agreement with Ref. 38. The width of these plateaus corresponds to  $\ell_{\text{step}}$ . In the regime  $\ell_{\text{step}} \lesssim 2\ell_B$  there is a qualitative change from the plateau-like to sine-like behavior of  $T_{20}$ , see Fig. 7(b). Thus, when  $\ell_{\text{step}} \lesssim 2\ell_B$ , the incoming current in  $L_0$  can be partitioned into valley-polarized currents in  $L_1$  ( $K$  valley) and  $L_2$  ( $-K$  valley) in any desired ratio by tuning the location of the  $p$ - $n$  junction. When  $\ell_{\text{step}} \lesssim 2\ell_B$ , mixing of Landau orbits on neighboring guiding centers gives rise to the conductance behavior shown in Fig. 7(b). Our results are in agreement with the simulations in Ref. 44.

In an experiment, one could measure the resulting valley polarization by utilizing the valley Hall effect<sup>6</sup>. This would require breaking the inversion symmetry, which can be modeled by a staggered sublattice potential of the form  $\pm\lambda_\nu \sum_i c_i^\dagger c_i$  in our system. Our results remain valid even after adding such a term to the Hamiltonian in Eq. (1) as long as  $\lambda_\nu < V_0$ . This condition ensures the presence of snake states in the system at  $E \approx 0$ .

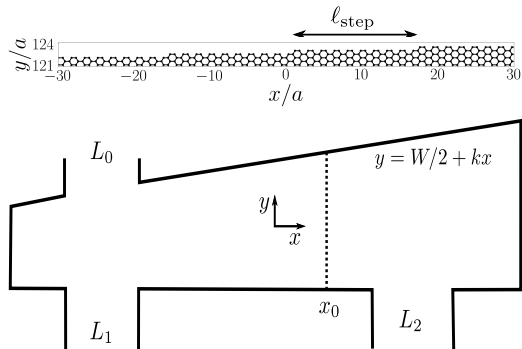
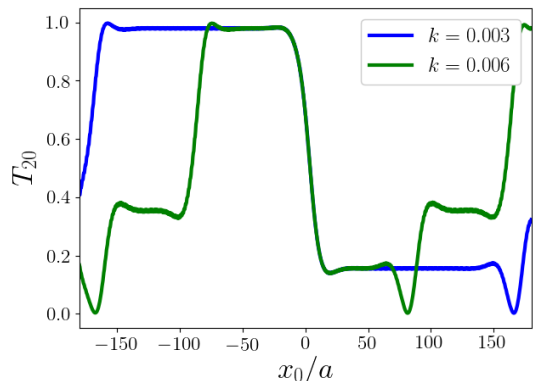
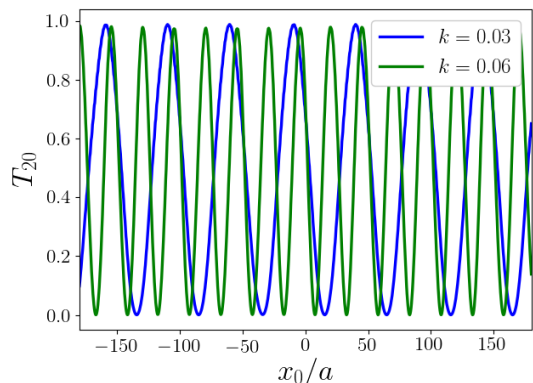


FIG. 6: Geometry of a device with a tilted staircase edge. Upper panel: zoom-in onto a part of the tilted upper edge displaying the staircase. The step length (length of the region of constant width  $W$ ) is denoted by  $\ell_{\text{step}}$ . Lower panel: a schematic of the device. The slope of the tilted edge  $k$  is related to  $\ell_{\text{step}}$ , e.g.  $k = 0.003$  corresponds to  $\ell_{\text{step}} \approx 166a$  while  $k = 0.03$  corresponds to  $\ell_{\text{step}} \approx 16a$ .



(a)



(b)

FIG. 7: Transmission  $T_{20}$  in a device with a tilted staircase edge as a function of the position of the  $p$ - $n$  interface  $x_0$  for different values of the slope  $k$ , see Fig. 6. (a) Plateau-like behavior of  $T_{20}$  as expected for  $\ell_{\text{step}} \gg 2\ell_B$ . (b) Sine-like behavior of  $T_{20}$  for  $\ell_{\text{step}} \lesssim 2\ell_B$ . In this figure  $L = 780a$ .

	geometry	$T_{10}$	$P_1$	$T_{20}$	$P_2$	notes
(a)		0.03	-	0.97	-1	$W = 246a$
		0.6	0.99	0.4	-0.99	$W = 247a$
		0.88	1	0.12	-1	$W = 248a$
(b)		0.0	-	1.0	-0.93	$L = 520a$
		1.0	0.93	0.0	-	$L = 521a$
(c)		0.48	1	0.52	-1	
(d)		1	1	0	-	W independent
(e)		0.02	-	0.98	-1	W independent

TABLE I: Transmissions  $T_{10}$  and  $T_{20}$  and polarizations  $P_1$  and  $P_2$  for different devices. The first column shows different sample geometries where the dashed line denotes the  $p$ - $n$  interface. (a) Transmissions for three different widths  $W$  for the same geometry as in Fig. 1, i.e. the  $p$ - $n$  interface meets armchair edges. The partitioning of the net transmission between  $T_{10}$  and  $T_{20}$  is a periodic function of  $W$  with period  $3a$  (or three hexagons across the width of the scattering region). (b) The  $p$ - $n$  interface meets edges of zigzag type. The two rows describe the zigzag/anti-zigzag configuration which lead to a different partitioning of the transmission. Note the changed position of the leads. (c) A triangular region is added to the lower edge (a zoom-in onto the tip is shown in the last column) to model different edge terminations. (d)–(e) Triangular regions added to the top and bottom edge.

## V. SUMMARY

In summary, we have demonstrated that a graphene  $p$ - $n$  junction in a uniform out-of-plane magnetic field can effectively function as a switchable valley filter. The valley polarization of the carriers in the outgoing leads is quite robust. Changing the edge termination at the  $p$ - $n$  interface can drastically modify the partitioning of the current into the two outgoing leads, but the outgoing current in both leads remains valley-polarized. We have also shown that in a device where one of the edges has many steps on the atomic scale, the partitioning of the current into two outgoing leads can be tuned by choosing the *location* of the  $p$ - $n$  junction. In such a device it will be possible to partition a valley-unpolarized incoming current into two streams of oppositely valley-polarized currents in two outgoing leads in any desired ratio.

## ACKNOWLEDGMENTS

We would like to acknowledge fruitful discussions with P. Makk, C. Handschin, and C. Schönberger. This work was financially supported by the Swiss SNF and the NCCR Quantum Science and Technology. Work by EJM was supported by the Department of Energy, Office of Basic Energy Sciences under grant DE FG02 84ER45118.

<sup>1</sup> K.S. Novoselov, A.K. Geim, S.V. Morozov, D. Jiang, Y. Zhang, S.V. Dubonos, I.V. Grigorieva, and A.A. Firsov, *Science* **306**, 666 (2004).  
<sup>2</sup> J.R. Schaibley, H. Yu, G. Clark, P. Rivera, J.S. Ross, K.L. Seyler, W. Yao, and X. Xu, *Nat. Rev. Mater.* **1**, 16055 (2016).  
<sup>3</sup> A. Rycerz, J. Tworzydło, and C.W.J. Beenakker, *Nat. Phys.* **3**, 172 (2007).  
<sup>4</sup> A.R. Akhmerov and C.W.J. Beenakker, *Phys. Rev. Lett.* **98**, 157003 (2007).  
<sup>5</sup> D. Xiao, M.C. Chang, and Q. Niu, *Rev. Mod. Phys.* **82**, 1959 (2010).  
<sup>6</sup> D. Xiao, W. Yao, and Q. Niu, *Phys. Rev. Lett.* **99**, 236809

(2007).  
<sup>7</sup> J. Li, K. Wang, K.J. McFaul, Z. Zern, Y.F. Ren, K. Watanabe, T. Taniguchi, Z.H. Qiao, and J. Zhu, *Nat. Nanotechnol.* **11**, 1060 (2016).  
<sup>8</sup> M. Sui, G. Chen, L. Ma, W. Shan, D. Tian, K. Watanabe, T. Taniguchi, X. Jin, W. Yao, D. Xiao, and Y. Zhang, *Nat. Phys.* **11**, 1027 (2015).  
<sup>9</sup> Y. Shimazaki, M. Yamamoto, I.V. Borzenets, K. Watanabe, T. Taniguchi, and S. Tarucha, *Nat. Phys.* **11**, 1032 (2015).  
<sup>10</sup> W. Yao, D. Xiao, and Q. Niu, *Phys. Rev. B* **77**, 235406 (2008).  
<sup>11</sup> D. Xiao, G.B. Liu, W. Feng, X. Xu, and W. Yao, *Phys.*

- Rev. Lett. **108**, 196802 (2012).
- <sup>12</sup> J.M. Pereira Jr., F.M. Peeters, R.N. Costa Filho, and G.A. Farias, J. Phys.: Condens. Matter **21**, 045301 (2009).
  - <sup>13</sup> M. Ramezani Masir, A. Matulis, and F. M. Peeters, Phys. Rev. B **84**, 245413 (2011).
  - <sup>14</sup> D. Moldovan, M. Ramezani Masir, L. Covaci, and F.M. Peeters, Phys. Rev. B **86**, 115431 (2012).
  - <sup>15</sup> S.-G. Cheng, J. Zhou, H. Jiang, and Q.-F. Sun, New Journal of Physics **18**, 103024 (2016).
  - <sup>16</sup> S. P. Milovanović and F. M. Peeters, App. Phys. Lett. **109**, 203108 (2016).
  - <sup>17</sup> M. Settnes, S. R. Power, M. Brandbyge, and A.-P. Jauho, Phys. Rev. Lett. **117**, 276801 (2016).
  - <sup>18</sup> Marko M. Grujić, Milan Ž. Tadić, and F.M. Peeters, Phys. Rev. Lett. **113**, 046601 (2014).
  - <sup>19</sup> M.O. Goerbig, Rev. Mod. Phys. **83**, 1193 (2011).
  - <sup>20</sup> J. E. Müller, Phys. Rev. Lett. **68**, 385 (1992).
  - <sup>21</sup> Sunghun Park and H.-S. Sim, Phys. Rev. B **77**, 075433 (2008).
  - <sup>22</sup> L. Oroszlány, P. Rakyta, A. Kormányos, C.J. Lambert, and J. Cserti, Phys. Rev. B **77**, 081403(R) (2008).
  - <sup>23</sup> T.K. Ghosh, A. De Martino, W. Häusler, L. Dell’Anna, and R. Egger, Phys. Rev. B **77**, 081404(R) (2008).
  - <sup>24</sup> E. Prada, P. San-Jose, and L. Brey, Phys. Rev. Lett. **105**, 106802 (2010).
  - <sup>25</sup> P. Carmier, C. Lewenkopf, and D. Ullmo, Phys. Rev. B **81**, 241406(R) (2010).
  - <sup>26</sup> P. Carmier, C. Lewenkopf, and D. Ullmo, Phys. Rev. B **84**, 195428 (2011).
  - <sup>27</sup> P. Rickhaus, P. Makk, M.H. Liu, E. Tóvári, M. Weiss, R. Maurand, K. Richter, and C. Schönenberger, Nat. Commun. **6**, 6470 (2015).
  - <sup>28</sup> C.W.J. Beenakker, A.R. Akhmerov, P. Recher, and J. Tworzydło, Phys. Rev. B **77**, 075409 (2008).
  - <sup>29</sup> Y. Liu, R.P. Tiwari, M. Brada, C. Bruder, F.V. Kusmartsev, and E.J. Mele, Phys. Rev. B **92**, 235438 (2015).
  - <sup>30</sup> J.R. Williams, L. DiCarlo, and C.M. Marcus, Science **317**, 638 (2007).
  - <sup>31</sup> M. Zarenia, J.M. Pereira, Jr., F.M. Peeters, and G.A. Farias, Phys. Rev. B **87**, 035426 (2013).
  - <sup>32</sup> T. Taychatanapat, J.Y. Tan, Y. Yeo, K. Watanabe, T. Taniguchi, and B. Özyilmaz, Nat. Commun. **6**, 6093 (2015).
  - <sup>33</sup> L.S. Cavalcante, A. Chaves, D.R. da Costa, G.A. Farias, and F.M. Peeters, Phys. Rev. B **94**, 075432 (2016).
  - <sup>34</sup> L. Cohnitz, A. De Martino, W. Häusler, and R. Egger, Phys. Rev. B **94**, 165443 (2016).
  - <sup>35</sup> C. Fräßdorf, L. Trifunovic, N. Bogdanoff, and P.W. Brouwer, Phys. Rev. B **94**, 195439 (2016).
  - <sup>36</sup> K. Kolasinski, A. Mreńca-Kolasińska, and B. Szafran, Phys. Rev. B **95**, 045304 (2017).
  - <sup>37</sup> D.A. Abanin and L.S. Levitov, Science **317**, 641 (2007).
  - <sup>38</sup> J. Tworzydło, I. Snyman, A.R. Akhmerov, and C.W.J. Beenakker, Phys. Rev. B **76**, 035411 (2007).
  - <sup>39</sup> L. Brey and H.A. Fertig, Phys. Rev. B **73**, 195408 (2006).
  - <sup>40</sup> C.W.J. Beenakker, Rev. Mod. Phys. **80**, 1337 (2008).
  - <sup>41</sup> C.W. Groth, M. Wimmer, A.R. Akhmerov, and X. Waintal, New J. Phys. **16**, 063065 (2014).
  - <sup>42</sup> S. P. Milovanović, M. Ramezani Masir, and F. M. Peeters, Appl. Phys. Lett. **105**, 123507 (2014).
  - <sup>43</sup> A.R. Akhmerov, J.H. Bardarson, A. Rycerz, and C.W.J. Beenakker, Phys. Rev. B **77**, 205416 (2008).
  - <sup>44</sup> C. Handschin, P. Makk, P. Rickhaus, R. Maurand, K. Watanabe, T. Taniguchi, K. Richter, M.-H. Liu, and C. Schönenberger, *submitted*.